Correspondence Between Simple 3-D MRI-Based Computer Models and *In-Vivo* EP Measurements in Swine With Chronic Infarctions

Mihaela Pop*, Maxime Sermesant, Tommaso Mansi, Eugene Crystal, Sudip Ghate, Jean-Marc Peyrat, Ilan Lashevsky, Beiping Qiang, Elliot McVeigh, Nicholas Ayache, and Graham A. Wright, *Member, IEEE*

***Abstract*—The aim of this paper was to compare several *in-vivo* electrophysiological (EP) characteristics measured in a swine model of chronic infarct, with those predicted by simple 3-D MRI-based computer models built from *ex-vivo* scans (voxel size $<1\,\mathrm{mm}^3$). Specifically, we recorded electroanatomical voltage maps (EAVM) in six animals, and ECG waves during induction of arrhythmia in two of these cases. The infarct heterogeneities (dense scar and border zone) as well as fiber directions were estimated using diffusion weighted DW-MRI. We found a good correspondence ($r = 0.9$) between scar areas delineated on the EAVM and MRI maps. For theoretical predictions, we used a simple two-variable macroscopic model and computed the propagation of action potential after application of a train of stimuli, with location and timing replicating the stimulation protocol used in the *in-vivo* EP study. Simulation results are exemplified for two hearts: one with noninducible ventricular tachycardia (VT), and another with a macroreentrant VT (for the latter, the average predicted VT cycle length was 273 ms, compared to a recorded VT of 250 ms).**

***Index Terms*—Arrhythmia, cardiac modeling, MRI.**

I. Introduction

ABNORMAL heart rhythms are often associated with chronic infarct scars and are a major cause (>85%) of sudden cardiac death [1]. One dangerous manifestation is ventricular tachycardia (VT), where a "reentry circuit" facilitates a fast re-excitation of the tissue. In such cases, the electrical wave loops fast around relatively large scars and through a so-called "isthmus," an abnormal pathway that contains viable myocytes interdigitated within nonconductive collagen [2]. The arrhythmogenic substrate is located at the border zone (BZ) of infarcts and is identified during long and invasive electrophysiological (EP) studies, which often use surface measurements and aggressive stimulation protocols to induce VT. Should this VT circuit fails to be interrupted, the propagation degenerates into lethal ventricular fibrillation (VF).

To complement the EP study, imaging methods (e.g., MRI) could identify the infarct extent, heterogeneities, as well as clinical characteristics that predict the patients susceptible to VT/VF [3]. Furthermore, 3-D computer modeling is a valuable tool that can be used in cardiac EP to understand the propagation of abnormal excitation waves [4]. Several efforts have been made to develop multiscale models that integrate imaging, microstructures, and biophysical details. Some researchers have focused on developing such models of small (rabbit) hearts [5], while others on large heart models using noisy *ex-vivo* fractional anisotropy from diffusion weighted DW-MR images of canine large hearts [6]. The latter used a 3-D heart model in combination with detailed, ionic equations to study macroreentrant VT inducibility, but this virtual study lacked any experimental validation. Alternatively, a simple and fast two-variable macroscopic formalism [7] could be used to model spirals [8] and macroreentrant waves [9], [10], the latter being associated with macroscopic circuits targeted for ablation therapies [1], [3].

In this paper, we explore simple modeling approaches combined with *in-vivo* EP measures to detect the extent of scars, as well as lead ECG waves (recorded during sinus rhythm and VT) in swine with chronic infarct. Our aim was to compare: 1) the scar extent in the 3-D MRI-model and in the electroanatomic voltage maps (EAVM); and 2) the predictions of (non)inducibility and VT cycle length given by a simple 3-D computer model, with the outcome of EP study.

II. Material and Methods

A. Electrophysiology Study

Myocardial infarction was generated in six swine by a 90-min balloon occlusion of coronary arteries, followed by reperfusion to create heterogeneous infarcts (in accordance to the protocol approved by Sunnybrook Research Institute, Toronto, CA). Four animals underwent the occlusion of left circumflex artery (LCX)

Manuscript received April 2, 2011; revised June 26, 2011 and August 11, 2011; accepted August 25, 2011. Date of publication September 15, 2011; date of current version November 18, 2011. This work was supported by the Canadian Institutes of Health Research under Grant MOP93531. *Asterisk indicates corresponding author.*

*M. Pop is with Sunnybrook Research Institute, Toronto, On M4N 3M5, Canada (e-mail: mpop@sri.utoronto.ca).

E. Crystal, S. Ghate, I. Lashevsky, B. Qiang, and G. A. Wright are with Sunnybrook Research Institute, Toronto, On M4N 3M5, Canada (e-mail: eugene.crystal@sunnybrook.ca; sghate@sri.utoronto.ca; ilan.lashevsky@sunnybrook.ca; bqiang@sri.utoronto.ca; gawright@sri.utoronto.ca).

M. Sermesant and N. Ayache are with Inria Asclepios team, 06 902 Sophia Antipolis, France (e-mail: maxime.sermesant@inria.fr; nicholas.ayache@inria.fr).

T. Mansi is with Siemens Corporate Research, Image Analytics and Informatics, Princeton, NJ 08540 USA (e-mail: Tommaso.mansi@tmansi.net).

J.-M. Peyrat is with Siemens Molecular Research, Oxford, OX1 2EP, U.K. (e-mail: jmpeyrat@gmail.com).

E. R. McVeigh is with Johns Hopkins University, Baltimore, MD 21202-2397 USA (e-mail: emcveigh@jhu.edu).

Color versions of one or more of the figures in this paper are available online at http://ieeexplore.ieee.org.

Digital Object Identifier 10.1109/TBME.2011.2168395

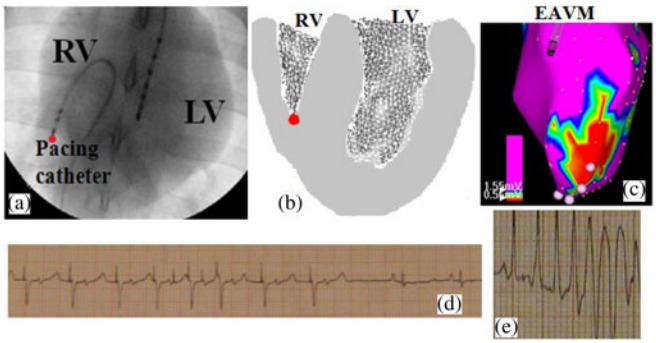

Fig. 1. Characteristics of the EP study. (a) Fluoroscopic view of the catheters inside the heart during the EP study. (b) Pacing location (red dot) in the 3-D model. (c) Example of endocardial EAVM (purple indicates healthy tissue). (d) ECG waves obtained in the noninducible VT case (LCX infarct) and (e) in the inducible VT case (LAD infarct).

TABLE I
PARAMETERS (BY ZONE) IN THE MATHEMATICAL MODEL

Zone	Model parameters		
	a	k	d
Healthy myocardium	0.112	8	3
Border zone (BZ)	0.2	2	1

and two had left anterior descendant artery (LAD) occluded. We demonstrated in another study that such heterogeneous areas are realistic, and evolution of acute infarct (in two days) to chronic stages (4–6 weeks) is similar to that in humans [11], as confirmed by histology.

The *in-vivo* EP studies in this paper were performed at ∼5 weeks postocclusion and involved: 1) the recording of EAVM on the endo- or epicardium using a CARTO-XP system (Biosense, Webster, CA) during normal sinus rhythm (nSR); and 2) in two swine, the inducibility of VT by following a precise stimulation protocol, which employed the application of a train of stimuli S1 that paced the heart fast (to override nSR), followed by several S2-S3 extra stimuli, delivered from the tip of a catheter inserted into the right ventricle RV [see Fig. 1(a)]; this location was also marked in the 3-D MRI computer model [see red dot in Fig 1(b)]. Fig. 1(c) shows an example of EAVM from a CARTO acquisition; the infarct is delineated by low voltages (red areas) in bipolar maps. We measured scar areas using the CARTO analysis software [1]. Fig. 1(d) and (e) shows examples of ECG waves recorded on paper in the two cases where VT induction was performed: one swine had LCX-infarct and the other had LAD-infarct. The LCX-infarct demonstrated noninducible VT after 13 pacing stimuli S1 = 550 ms, followed by two S2 extra stimuli at 400 ms and one S3 at 300 ms; which failed to induce VT, and consequently, the nSR was recorded again [see Fig. 1(d)]. For the LAD-infarct heart, the VT was induced after pacing with eight stimuli S1 = 800 ms, followed by three S2 extra stimuli at 300 ms, inducing VT. Several VT cycles were recorded on paper, of approximately 250 ms each [see Fig. 1(e)]. We did not acquire CARTO maps during the two VT inducibility studies.

B. Construction of the 3-D MRI-Based Heart Model

At the completion of *in-vivo* EP studies, the hearts were explanted, preserved few days in formalin, and MR-imaged for anatomy, scar characterization, and fiber directions using DW-MR. The 3-D model was constructed from ADC maps (apparent diffusion coefficient), which were then used to segment the heart into three zones: healthy tissue, BZ, and scar. Surface meshes were created from the 3-D anatomy MR scans, and tetrahedral meshes were generated with TetGen package. We measured the scar areas in 3-D MR model to compare them with areas from the EAVM.

C. Mathematical Model

We used the simple two-variable model developed by Aliev and Panfilov, which is based on reaction-diffusion type of equations [7]. We solve for the action potential using the finite-element method, with an explicit Euler time integration scheme [12]. This macroscopic model accounts for heart anisotropy via a diffusion tensor D (which depends on tissue "bulk" conductivity d). For instance, the value in the anisotropy ratio is set to 0.14 for a wave propagating almost 2.7 times as fast along the fiber as in the transverse direction.

Some input values for model parameters were taken from our recent optical imaging *ex-vivo* study [13] in infarcted swine hearts, and they were assigned by zones. The restitution curves in that study were generated by plotting APD90 (ms) versus cycle length, (CL in ms), at different pacing frequencies (e.g., in the normal zone, measured APD90 = 0.218 × CL +151 and computed APD90 = 0.213 × CL +160). The fits were done using *ex-vivo* optical measures, but the AP characteristics at four weeks are close to those found by others [2] at similar times. The values for a (tuning the duration of AP), k (tuning the up-stroke of AP) and the normalized conductivity d were set as in Table I. Note that d was set to 0 in the scar. The rest of the parameters (i.e., ε and μ) were set as in [8].

The stimulation in the heart model was achieved as follows: 1) the nSR was simulated by applying a 5-ms duration square pulse (note $V = 1$, since the model output has normalized AP values), simultaneously on the endocardial surfaces of RV and LV to mimic activation from Purkinje sites; and 2) the pacing was simulated by applying a train of stimuli (5-ms square pulses, $V = 1$) replicating the duration and timing as in EP study, as well as the catheter tip location.

A time step of 5×10^{-5} s yielded a computational time of 50 min for 1 s of simulated heart cycle on a regular PC. The mesh for LCX-infarct heart had 212 678 elements, whereas for the LAD-infarct heart the mesh had 245 591 elements (average element size 1 mm, which is sufficient to simulate macroreentrant VT, as demonstrated in the *Appendix*).

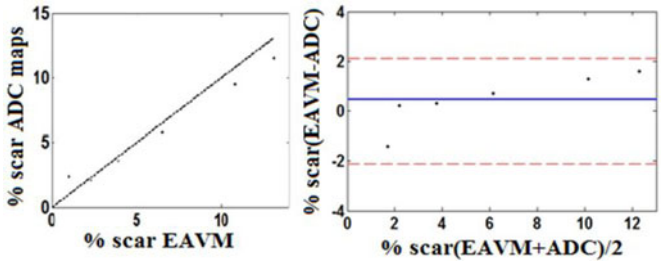

Fig. 2. Quantitative analysis for % area scar delineated by EAVM and ADC-MRI maps. (left) Correlation plot. (Right) Bland–Altman plot (blue line corresponds to the mean value, and red line to $\pm$ 2 S.D).

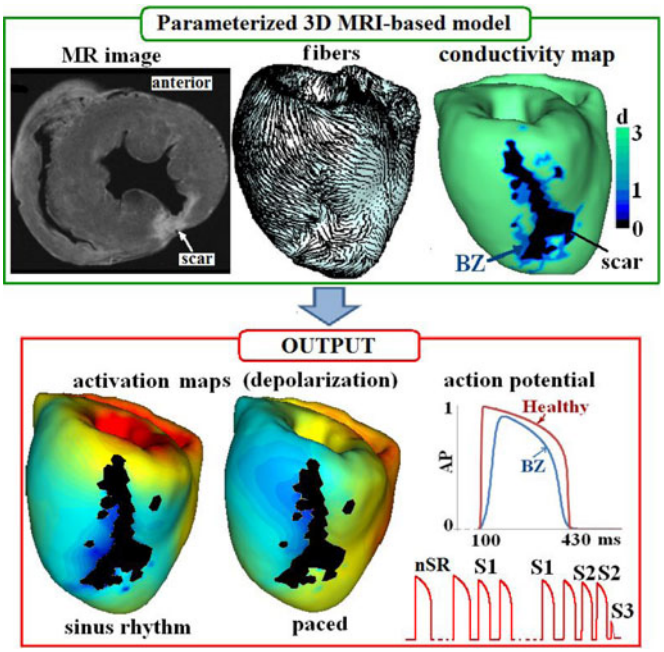

Fig. 3. (Upper panel) 3-D MRI-based model for the LCX-infarct heart (from segmented ADC maps, and fibers from DT-MRI), together with input 3-D conductivity map (with scar in black, healthy in green, BZ in light-blue). (Lower panel) Isochronal maps for depolarization times (color scale corresponding to early activation times in red and late activation times in blue) during nSR and pacing, and computed AP before and after the S1-S2-S3 train (resulting in noninducible VT).

III. Results

A. Comparison Between Scar Area in EAVM and MRI Maps

Fig. 2 shows the results obtained after comparing the scar extent measured on the endocardium or epicardium, in the segmented 3-D ADC maps and in the EAV maps, respectively.

The plot shown in Fig. 2 (left) yielded very good correlation ($r = 0.9$) between the % scar area delineated in these maps, with EAVM slightly overestimating areas. The Bland–Altman analysis [see Fig. 2 (right)] showed no bias between the methods.

B. Assessment of VT Inducibility in the 3-D Model

The results shown in Fig. 3 were obtained with the LCX-infarct, and illustrate construction and parametrization of the 3-D MRI-based computer model, together with an example of theoretical propagation of AP computed on this heart. The upper panel shows a 2-D axial view through the 3-D ADC with elevated ADC values in the scar, the fiber directions from DW-MRI (with severe fibers' disarray in scar), and the 3-D d-map corresponding to the MRI-based model (d is set to zero in the scar shown in black and has reduced values in BZ). The model predicted correctly noninducible VT for this case.

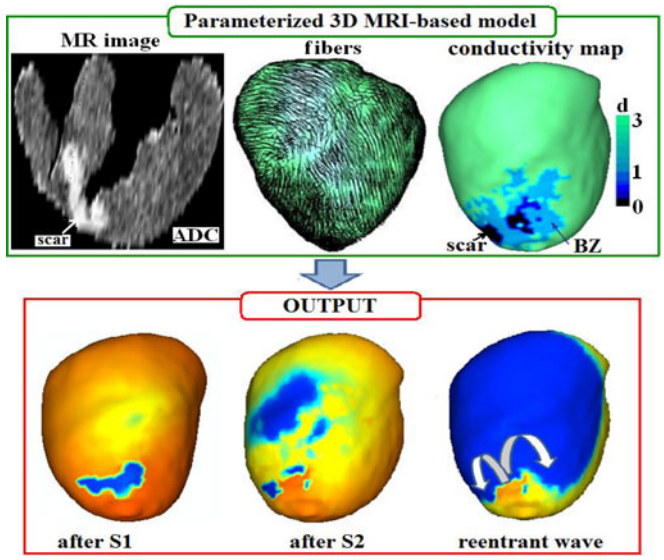

Fig. 4. (Upper panel) 3-D MRI-based parameterized model for the LAD-infarct heart from ADC maps, together with a top view through the mesh and the input 3-D d-map by zone. (Lower panel) Simulated isochronal maps after S1, S2, and reentrant VT wave propagating around the dense scars (in the directions indicated by the white arrows).

Similarly, Fig. 4 presents results from the model obtained for the LAD infarct. Different geometry of scar and BZ leads to inducible VT; VT wave looped around scars with a cycle length of 273 ms (compared to 250 ms in the EP study).

IV. Discussion and Future Work

Prior to integration into clinical applications, 3-D MRI-based computer models have to be validated using measures selected to reflect EP phenomena at spatio-temporal scales similar to those considered in simulations [4]. A first step toward this goal is the construction of 3-D models from large animal models relevant to human studies and the comparison between the model output and *in-vivo* EP measurements.

In this study, we found that ADC maps from DW-MRI identify very well the scar areas in swine hearts with chronic infarcts and can provide additional information than the surfacic EAVM, like the transmural extent of scar and BZ. Moreover, the EAVM overestimates the scar area, likely due to their poorer spatial resolution compared to high-resolution MR images. Although we carefully preserved the hearts, small deformation and shrinking in formalin could contribute to the difference between the two methods (*in-vivo* EP versus *ex-vivo* MRI). However, the 3-D model was built from *ex-vivo* scans because DW-MRI is not currently suitable to clinical investigations due to motion, image noise, and long scans. Our model is realistic for

computational purposes because it integrates the fibers. Another study combining *in-vivo* EP with *ex-vivo* contrast-enhanced MR [14] used invasive multielectrodes that destroyed tissue (hampering DW-MRI); however, that study has the advantage that it mapped the depolarization times during VT (from multiple electrode points on the epicardium, simultaneously).

We acknowledge that our model is simple compared to ionic models that capture correctly restitution properties and functional VT/VF phenomena like in acute ischemia [4] or in diffuse fibrosis [15] (when spiral waves rotate around small cores). Our experimental model was developed to reflect characteristics of macroscopic reentries in the early chronic stage of the infarction (4–5 weeks). This is the time when the scar stabilizes and patients are suitable for ablation therapies; most of these patients present with anatomic macroreentrant VT due to relatively large circuits [1], [3]. Our simulations were performed for two infarcted hearts: with noninducible VT and with inducible VT, successfully predicting the outcome as in the *in-vivo* EP studies. Both cases are clinically relevant, since many patients with prior infarct do not develop VT/VF and inappropriately undergo implantation of cardioverter devices. For the VT-inducible heart, the average predicted VT cycle length was slightly longer (by 23 ms) compared to the recorded cycle length, possibly due to input model parameters assigned to different zones. However, we demonstrated in [13] very good correspondence between our classification and the extent of scars in histological images. Also, in a recent study, we reported good agreement between infarct classifications obtained using contrast-enhanced MRI methods (clinically used) and the DW method. This gives us confidence that our predictions using 3-D models built using contrast-based methods will give similar results.

We parameterized the model using global values for *k, a*, and *d* by zone, but these zones could be refined in smaller subzones with different *d*-values. A limitation is that our *d*-values were derived from an *ex-vivo* optical study. Thus, further experimentation is needed to assess *in-vivo* restitution curve; such step should involve endo- or episurface mapping under pacing conditions and computing *d*-maps from depolarization maps; such *in-vivo* restitution curve could be obtained using monophasic AP catheters [16], and would definitely allow a more precise customization of *a* and *k*.

APPENDIX

We used a thin rectangular slab (3 cm $\times$ 3 cm $\times$ 0.5 cm), with 1-mm element size. Fig. 5 shows results of a macroreentrant wave (VT = 318 ms) that looped around scars through an isthmus. A convergence test for time steps (using 1×10^{-4}, 5×10^{-5}, 3.5×10^{-5}, and 2×10^{-5} s) resulted in approximately 3% difference in APD90 values, when using 5×10^{-5} s compared to 2×10^{-5} s. Thus, 5×10^{-5} s seems sufficient for modeling VT using such meshes. For space scale, VT cycle was 14 ms faster using a mesh with 0.5-mm element size than for 1-mm size.

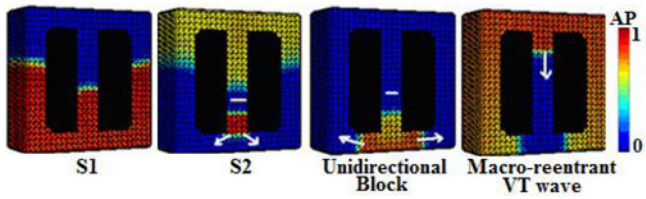

Fig. 5. Macroreentrant VT in a simple rectangular slab: snapshots at different times during depolarization (red) and recovering (blue) phase following S1 and S2, which induced a unidirectional propagation in the isthmus, and a VT wave looping around scars (black).

REFERENCES

[1] W. G. Stevenson, "Ventricular scars and VT tachycardia," *Trans. Am. Clin. Assoc.*, vol. 120, pp. 403–412, 2009.
[2] P. C. Ursell, P. I. Gardner, A. Albala, J. Fenoglio, and A. Wit, "Structural and EP changes in the epicardial border zone of canine myocardial infarcts during healing," *Circulation Res.*, vol. 56, pp. 436–451, 1985.
[3] D. Bello, D. S. Fieno, R. J. Kim, F. S. Pereles, R. Passman, G. Song, A. H. Kadish, and J. J. Goldberger, "Infarct morphology identifies patients with substrate for sustained ventricular tachycardia," *J. Am. College Cardiology*, vol. 45, no. 7, pp. 1104–1108, 2005.
[4] R. H. Clayton and A. V. Panfilov, "A guide to modelling cardiac electrical activity in anatomically detailed ventricles (review)," *Prog. Biophys. Molecular Biol.*, vol. 96, no. 1–3, pp. 19–43, 2008.
[5] M. Bishop, G. Plank, R. A. B. Burton, J. E. Schneider, D. J. Gavaghan, V. Grau, and P. Kohl, "Development of an anatomically detailed MRI-derived rabbit ventricular model and assessment of its impact on simulations of electrophysiological function," *Am. J. Physiol.: Heart Circulation Physiol.*, vol. 298, pp. H699–H718, 2009.
[6] F. Vadakkumpadan, L. Rantner, B. Tice, P. Boyle, A. Prassl, E. Vigmond, G. Plank, and N. Trayanova, "Image-based models of cardiac structure with applications in arrhythmia and defibrillation studies," *J. Electrocardiology*, vol. 42, no. 2, p. 157.e1–157.e10, 2009.
[7] R. Aliev and A. V. Panfilov, "A simple two variables model of cardiac excitation," *Chaos, Soliton Fractals*, vol. 7, no. 3, pp. 293–301, 1996.
[8] M. P. Nash and A. V. Panfilov, "Electromechanical model of the excitable tissue to study reentrant cardiac arrhythmias," *Prog. Biophys. Molecular Biol.*, vol. 85, pp. 501–510, 2004.
[9] S. Sinha, K. Stein, and D. Christini, "Critical role of inhomogeneities in pacing termination of cardiac reentry," *Chaos*, vol. 12, pp. 893–901, 2002.
[10] M. Pop, M. Sermesant, M. Peyrat, E. Crystal, A. Dick, and A. Wright, "Anatomic reentry: Insights from a study in a simple 3D anisotropic wedge model," *Int. J. Bioelectromagnetism*, vol. 11, no. 1, pp. 133–151, 2011.
[11] N. R. Ghugre, V. Ramanan, M. Pop, Y. Yang, J. Barry, B. Qiang, K. Connelly, A. J. Dick, and G. A. Wright, "Quantitative tracking of edema, hemorrhage and microvascular obstruction after acute myocardial infarction by MRI," *Magn. Reson. Med.*, vol. 66, no. 4, pp. 1129–1141, Oct. 2011.
[12] M. Sermesant, H. Delingette, and N. Ayache, "An electromechanical model of the heart for image analysis and simulation," *IEEE Trans. Med. Imag.*, vol. 25, no. 5, pp. 612–625, May 2006.
[13] M. Pop, M. Sermesant, G. Liu, J. Relan, T. Mansi, A. Soong, M. V. Truong, P. Fefer, E. R. McVeigh, H. Delingette, A. J. Dick, N. Ayache, and G. A. Wright, "Construction of 3D MRI-based computer models of pathologic hearts, augmented with histology and optical imaging to characterize the action potential," *Med. Image Anal.*, 2011, to be published.
[14] H. Ashikaga, T. Sasano, J. Dong, M. M. Zviman, R. Evers, B. Hopenfeld, V. Castro, R. H. Helm, T. Fickfeld, S. Nazarian, J. K. Donahue, R. D. Berger, H. Calkins, R. M. Abraham, E. Marban, A. C. LArdo, E. R. McVeigh, and H. Halperin, "MR-based anatomical analysis of scar-related VT: implications for catheter ablation," *Circulation Res.*, vol. 101, no. 9, pp. 939–947, 2007.
[15] K. H. J. Ten Tusscher and A. Panfilov, "Influence of diffuse fibrosis on wave propagation in human ventricular tissue," *Europace*, vol. 9, pp. 38–45, 2007.
[16] S. C. Hao, D. J. Christini, K. M. Stein, P. N. Jordan, S. Iwai, O. Bramwell, S. M. Markowitz, S. Mittal, and B. Lerman, "Effect of beta-adrenergic blockade on dynamic electrical restitution *in-vivo*," *Amer. J. Physiol.*, vol. 287, pp. H390–H394, 2004.